HHS Public Access

Author manuscript

Cell Rep. Author manuscript; available in PMC 2020 February 18.

Published in final edited form as:

Cell Rep. 2019 January 15; 26(3): 518–528.e6. doi:10.1016/j.celrep.2018.12.070.

Maintenance of Cardiolipin and Crista Structure Requires Cooperative Functions of Mitochondrial Dynamics and Phospholipid Transport

Rieko Kojima[1], **Yuriko Kakimoto**[1], **Shiina Furuta**[1,5], **Kie Itoh**[2], **Hiromi Sesaki**[2], **Toshiya Endo**[3,4], **Yasushi Tamura**[1,6,*]

[1]Department of Material and Biological Chemistry, Faculty of Science, Yamagata University, 1-4-12 Kojirakawa-machi, Yamagata, Yamagata, 990-8560, Japan

[2]Department of Cell Biology, The Johns Hopkins University School of Medicine, 725N Wolfe St., Baltimore, MD, 21205, USA

[3]Faculty of Life Sciences, Kyoto Sangyo University, Kamigamo-motoyama, Kita-ku, Kyoto 603-8555, Japan

[4]Institute for Protein Dynamics, Kyoto Sangyo University, Kamigamo-motoyama, Kita-ku, Kyoto 603-8555, Japan

[5]Present address: Department of Biological Science, Graduate School of Science, Osaka University, 1–1 Matikaneyama, Toyonaka, Osaka, 560-0043, Japan

[6]Lead Contact

SUMMARY

Mitochondria are dynamic organelles that constantly fuse and divide to maintain their proper morphology, which is essential for their normal functions. Energy production, a central role of mitochondria, demands highly folded structures of the mitochondrial inner membrane (MIM) called cristae and a dimeric phospholipid (PL) cardiolipin (CL). Previous studies identified a number of factors involved in mitochondrial dynamics, crista formation, and CL biosynthesis, yet it is still enigmatic how these events are interconnected and cooperated. Here, we first report that mitochondrial fusion/division dynamics is important to maintain CL abundance. Second, our genetic and biochemical analyses revealed that intra-mitochondrial PL transport plays an important role in crista formation. Finally, we show that simultaneous defects in MIM fusion and intra-mitochondrial PL transport cause a drastic decrease in crista structure, resulting in decreased CL levels. These results expand our understanding of the integrated functional network among the PL transport, crista formation, and CL biogenesis.

*Correspondence: tamura@sci.kj.yamagata-u.ac.jp.

Author Contributions

HS, TE, RK, and YT designed the study. RK and YT performed the most experiments. KI helped to perform a part of the EM analyses. SF and YK performed a part of phospholipid analyses. HS, TE, RK, and YT wrote the paper.

DECLARATION OF INTERESTS

The authors declare no competing interests.

SUPPLEMENTAL INFORMATION

Supplemental Information includes three figures can be found with this article online.

INTRODUCTION

Mitochondria, power plants in eukaryotic cells, produce most cellular ATP molecules by oxidative phosphorylation, as well as reactive oxygen species (ROS) as bi-products. To prevent accumulation of ROS-mediated oxidative damage of mitochondrial contents including mitochondrial DNA, mitochondria constantly exchange their contents through their fusion and division processes. For efficient ATP production, the mitochondrial inner membrane (MIM) is folded inwards to form crista structures for maximizing its surface area. Cardiolipin (CL), a mitochondria-specific phospholipid (PL), also plays critical roles in ATP production through stabilizing the respiratory chain supercomplexes (Böttinger et al., 2012; Claypool et al., 2008; Pfeiffer et al., 2003; Zhang et al., 2005). In addition, CL is also important for other mitochondrial functions including mitochondrial fusion/division dynamics (DeVay et al., 2009; Joshi et al., 2012; Kameoka et al., 2018), mitochondrial protein import (Gebert et al., 2009; Kutik et al., 2008; Malhotra et al., 2017; Sauerwald et al., 2015; Tamura et al., 2009) and regulation of mitophagy (Chu et al., 2013; Shen et al., 2017). In *Saccharomyces cerevisiae,* CL is synthesized via a series of modifications of phosphatidic acid (PA), the precursor PL generated in the ER. To synthesize CL, PA is first transported to the MIM, where CL synthetic enzymes are located. On the matrix side of the MIM, Tam41, mitochondrial CDP-diacylglycerol (DAG) synthase converts PA to CDP-DAG by using a nucleotide CTP (Tamura et al., 2013). Then, Pgs1, PGP synthase substitutes glycerol for the CDP moiety of CDP-DAG, producing phosphatidylglycerol phosphate (PGP) (Chang et al., 1998a). Gep4, PGP phosphatase dephosphorylates PGP to form phosphatidylglycerol (PG) (Osman et al., 2010). Crd1, CL synthase couples PG and CDP-DAG to generate CL (Tuller et al., 1998; Chang et al., 1998b). Finally, CL is matured through remodeling of its fatty acid chains by Cld1 CL-specific phospholipase and Taz1 acyltransferase (Beranek et al., 2009; Gu et al., 2004).

In addition to these CL synthetic enzymes, PL transfer proteins play essential roles in CL biosynthesis. A highly conserved protein complex, Ups1-Mdm35 is a lipid transfer machinery present in the mitochondrial intermembrane space (IMS) (Osman et al., 2009; Potting et al., 2010; Sesaki et al., 2006; Tamura et al., 2009, 2010). Biochemical and structural studies revealed that the Ups1-Mdm35 complex specifically recognizes the head group of PA and transfers PA from the MOM to MIM (Connerth et al., 2012; Watanabe et al., 2015; Yu et al., 2015). The Ups1-Mdm35 complex thus contributes to CL biosynthesis by delivering PA to the MIM, where the CL synthetic enzymes are located. Ups2, a Ups1 homologue, also forms a complex with Mdm35 and mediates phosphatidylserine (PS) transfer from the MOM to MIM, thereby contributing to phosphatidylethanolamine (PE) synthesis in mitochondria since PS synthesized outside mitochondria is converted to PE by Psd1 PE synthase in the MIM (Aaltonen et al., 2016; Miyata et al., 2016). In fact, loss of Ups1 or Ups2 leads to a decrease in the CL or PE level, respectively. CL and PE, both of which tend to form a nonbilayer membrane structure, are functionally redundant in part and the simultaneous loss of enzymes involved in the biosynthesis of CL and PE is synthetic lethal (Gohil et al., 2005). Therefore, one can naturally expect that simultaneous loss of Ups1 and Ups2 would cause a severe growth defect. However strangely, this is not the case; *ups1*Δ*ups2*Δ cells grow almost normally and contain a comparable amount of CL to that of

wild-type cells (Tamura et al., 2009). These findings indicate that defective CL synthesis due to the absence of Ups1 is restored by the additional loss of Ups2. One explanation for this observation could be that the decreased PE level in mitochondria rather than loss of Ups2 would activate other pathway(s) to replenish CL in the absence of Ups1 (Miyata et al., 2017). Puzzlingly, CL synthetic enzymes such as Tam41 and Pgs1 are dispensable for CL synthesis when Ups1 is absent (Connerth et al., 2012). These findings collectively suggest that there are still unknown pathways and/or factors important for CL biosynthesis.

We reasoned that the unknown factors that can compensate the defects in PL transport for the CL and PE synthesis would become critical for cell growth in the absence of Mdm35, which is the functional binding partner for both Ups1 and Ups2. In this work, we focused on Mgm1, a dynamin-related GTPase that mediates the fusion of the MIM (Sesaki et al., 2003; Wong et al., 2000) and the formation of lamellar cristae, because it is reported to genetically interact with the *MDM35* gene (Hoppins et al., 2011; Harner et al., 2016). Interestingly, simultaneous loss of Mdm35 and Mgm1, but not another mitochondrial protein for the MOM fusion Fzo1(Hermann et al., 1998), led to severe defects in growth and crista formation, suggesting that Mdm35 plays an overlapping function with Mgm1 in crista formation rather than mitochondrial fusion (Sesaki et al., 2003; Wong et al., 2000). Indeed, we confirmed that loss of Mdm35 alone causes a decrease in the crista structure. In addition, we show that the CL level is significantly decreased when crista formation is strongly impaired. These findings indicate that mitochondrial inner membrane fusion and intra-mitochondrial PL transport collectively contribute to the formation of normal MIM structures, which are prerequisite for the CL maintenance. These findings point to the importance of the previously overlooked relationship among the mitochondrial dynamics, PL transport, crista structure, and CL biogenesis.

Results and Discussion

Mgm1 is critical for cell growths when Mdm35 is absent—To gain insight into the "alternative" CL synthetic pathway that is activated upon inactivation of the Ups proteins, we investigated the genes that genetically interact with *MDM35* using the genetic interactome information available at the *Saccharomyces* genome database (http://www.yeastgenome.org/). Among a number of the candidate genes, we focused on *DNM1* and *MGM1*, which are involved in mitochondrial division and fusion, respectively, since these genetic interactions could point to uncharacterized roles, if any, of mitochondrial dynamics in the cellular phospholipid (PL) homeostasis.

We first tried to confirm if Dnm1 is indeed important for the growth of *mdm35*Δ cells as reported previously (Hoppins et al., 2011). To this end, we combined the *mdm35*Δ mutation with the *dnm1*Δ mutation and compared their cell growth with that of wild-type or the single-deletion mutant strains. As controls, we also created the *dnm1*Δ mutant strains with the *ups1*Δ or *ups2*Δ mutation. The *ups1*Δ strain showed defective cell growth whereas both the *ups2*Δ and *mdm35*Δ strains grew normally at 30°C and 37°C on a fermentable medium, YPD (Fig. 1A) (Tamura et al., 2009, 2010), although *mdm35*Δ cells grew more slowly than that of wild-type at low temperature 23°C (Potting et al., 2010). The *dnm1*Δ mutation hardly affected the growth of the single-deletion *ups1*Δ, *ups2*Δ and *mdm35*Δ strains on the

fermentable medium, YPD, whereas it caused synthetic growth defects with the *ups2*Δ or *mdm35*Δ mutation on a nonfermentable medium, YPLac at 37°C. This suggests that mitochondrial division becomes important when Ups2 or Mdm35 is absent under non-fermentable conditions and at elevated temperature (Fig. 1B).

Next, we attempted to confirm if *MGM1* genetically interacts with *MDM35.* The phenotypes caused by impaired mitochondrial fusion, such as fragmented mitochondria, growth defects and loss of mitochondrial DNA (mtDNA), can be restored by additional loss of a mitochondrial division factor like Dnm1 (Lee et al., 2012; Sesaki and Jensen, 2001; Sesaki et al., 2003). We thus deleted the *MGM1* gene together with the *DNM1* gene to eliminate possible secondary effects associated with such strong phenotypes seen in cells defective in the mitochondrial fusion. As a control, we tested the effects of lack of Fzo1, which is another mitochondrial fusion protein localized in the MOM (Hermann et al., 1998), although genetic interactions have not been reported for *MDM35* with *FZO1.* The triple-deletion *mgm1*Δ*dnm1*Δ*mdm35*Δ cells showed severe growth defects under any conditions we tested, including both fermentable and non-fermentable media, even severer than those of *mgm1*Δ*dnm1*Δ*ups1*Δ cells. In contrast, the *fzo1*Δ mutation only mildly affected the growths of cells lacking Mdm35 (Fig. 1C, D). Therefore, Mgm1, not Fzo1, is crucial for the restoration of the growth defects arising from the block of the Ups1/2 mediated PA and PS transports across the IMS by the *MDM35* deletion.

Cardiolipin is significantly decreased when both Mgm1 and Mdm35 are lacking—The strong negative-genetic interactions between the *MDM35* and *MGM1* genes suggest that Mgm1 is required for the restoration of the CL level in *mdm35*Δ cells. To test this notion, we analyzed the effects of the *ups1*Δ, *ups2*Δ or *mdm35*Δ mutation on PL compositions of wild-type, *dnm1*Δ, *fzo1*Δ*dnm1*Δ , and *mgm1*Δ*dnm1*Δ cells. Total PLs were prepared from those yeast cells cultivated in YPD containing ^{32}Pi and analyzed by thin-layer chromatography (TLC). As we reported previously, the *ups1*Δ strain showed decreased CL but normal PE levels whereas *ups2*Δ and *mdm35*Δ strains contained nearly normal CL but decreased PE levels (Fig. 2). The levels of other major PLs such as phosphatidylserine, phosphatidylinositol, and phosphatidylcholine were not drastically altered among the mutant cells although the levels of a minor PL, phosphatidic acid decreased when mitochondrial fusion/division dynamics was defective. The *dnm1*Δ mutation slightly decreased the CL levels for the strains with the *ups1*Δ or *ups2*Δ background, not for wild-type strain, and these decreases appeared additive in the *dnm1*Δ*mdm35*Δ strain. Nevertheless, the CL level was significantly restored in *dnm1*Δ*mdm35*Δ strain as compared with the *dnm1*Δ*ups1*Δ strain. The *dnm1*Δ mutation did not affect the levels of PE for the strains with or without *ups1*Δ, *ups2*Δ or *mdm35*Δ background at all. These data suggest that Dnm1 has a minor role in maintaining the normal CL abundance. Interestingly, we found that CL levels decreased to ~50% in the *fzo1*Δ*dnm1*Δ and *mgm1*Δ*dnm1*Δ strains, but not in the *dnm1*Δ strain. We further noticed that the CL and PE levels were significantly lower in *fzo1*Δ and *mgm1*Δ cells like those of ρ^0 cells, suggesting that the presence of mtDNA is critical to maintain normal levels of CL and PE (Fig. S1). This may indicate an uncharacterized role of mitochondrial fusion/division dynamics in the maintenance of the normal CL levels.

The decreased CL levels could be a cause for the impaired cell growth of *fzo1*Δ*dnm1*Δ*ups2*Δ and *fzo1*Δ*dnm1*Δ*mdm35*Δ under non-fermentable conditions (Fig. 1D) because concomitant decreases in levels of functionally redundant CL and PE are known to cause synthetic growth defects (Gohil et al., 2005). In addition, we noticed that the loss of Ups1 further decreases the CL levels in the *fzo1*Δ*dnm1*Δ and *mgm1*Δ*dnm1*Δ strains to ~10% as compared with that of the wild-type strain (Fig. 2). These findings indicate that impaired mitochondrial fusion/division events could lead to the decrease in the CL levels irrespective of the normal PA transport by Ups1. It should be emphasized that the *mdm35*Δ mutation did not restore the CL level at all in the strains with the *mgm1*Δ*dnm1*Δ background whereas it did for *the fzo1*Δ*dnm1*Δ background.

In summary, despite the overlapping function of Fzo1 and Mgm1 in mitochondrial fusion, our genetic and biochemical analyses showed that Mgm1 but not Fzo1 is critical for the cell growth and CL abundance of the strain lacking Mdm35. These data point out the crucial role of Mgm1 in the maintenance of CL abundance when Mdm35 is absent and suggest that Mgm1, but not Fzo1, has an overlapping function with Mdm35 in the CL biogenesis.

Mgm1 and Mdm35 play an overlapping role in crista formation—Electron tomographic analyses revealed the presence of two distinct types of crista structures, lamellar and tubular cristae, and lamellar crista was suggested to be generated by the fusion of two distinct MIMs by Mgm1 after fusion of MOMs (Harner et al., 2016). In contrast, tubular crista formation may instead require the import of proteins and PLs into the MIM, although this idea has not been experimentally tested yet. The MICOS complex at the crista junctions (CJs) appears to be involved in the formation of both the lamellar and tubular cristae (Harner et al., 2011; Hoppins et al., 2011; von der Malsburg et al., 2011; Rabl et al., 2009; Tarasenko et al., 2017). Taking this knowledge into consideration, we reasoned that simultaneous loss of Mgm1, involved in lamellar crista formation, and Mdm35, involved in tubular cristae formation through PL transport, may lead to impairment of the total crista formation and thereby result in severe growth defects and decreased CL levels. To test this idea, we analyzed the ultrastructure of the MIM in the presence or absence of Mdm35 and/or mitochondrial dynamics proteins Fzo1, Dnm1, and Mgm1 by electron microscopy (Fig. 3A). Consistent with previous studies, the electron micrographs showed that clear crista structures are present in *fzo1*Δ*dnm1*Δ and in *mgm1*Δ*dnm1*Δ cells (Fig. 3B) (Harner et al., 2016; Sesaki et al., 2003). We also confirmed the previous observation that septa structures were observed more frequently in the mitochondria without Fzo1 than in those without Mgm1 (Fig. 3A, B) (Harner et al., 2016). Interestingly, loss of Mdm35 led to a decrease in crista structures, suggesting the potential role of intramitochondrial PL transports in crista formation. Strikingly, the MIM structure was drastically altered when both *MDM35* and *MGM1* were deleted in the *dnm1*Δ background, and even empty mitochondria without internal MIM structures were frequently detected (Fig. 3A, B). Such severe alterations in the MIM structure were not seen in *fzo1*Δ*dnm1*Δ*mdm35*Δ cells, suggesting that Mdm35 and Mgm1 but not Fzo1 play an overlapping function in crista formation. In addition, these results clearly pointed out that Mgm1 can generate lamellar crista structure even without MOM-fusion events. Although how Mgm1 contributes to lamellar crista formation without MOM fusion is unclear at this point, the MIM may divide in a Dnm1-independent manner

(Messerschmitt et al., 2003) and lamellar crista may be generated by Mgm1-dependent fusion of the two distinct MIMs. Identification of such factors that mediate the MIM division would be of important for understanding the mechanism of crista formation.

Based on these observations, we conclude that the three key factors i.e. Mgm1, MICOS and Mdm35 (or intramitochondrial PL transport) are functionally interconnected to form normal crista structures (Fig. 3C and D). As summarized in Fig. 3C, defective intramitochondrial PL transport due to the Mdm35 loss negatively affects crista formation even though both Mgm1 and MICOS are functional (Fig. 3B and C, row 2). On the other hand, either the *mgm1*Δ*dnm1*Δ or *mic60*Δ mutation does not affect crista formation to that extent although CJs are largely missing in the absence of Mic60 (Körner et al. 2009; Harner et al., 2011; Hoppins et al., 2011; von der Malsburg et al., 2011, Fig. 3 C lines 3 and 4). Therefore, functions of Mgm1 and MICOS are not sufficient to generate normal crista structures in the absence of Mdm35, or in other words, intramitochondrial PL transport contributes to Mgm1- and/or MICOS-dependent crista formations.

Interestingly, intramitochondrial PL transport seems to act on the MICOS-dependent crista formation rather than Mgm1-dependent one because simultaneous deletions of *MICOS* (*MIC10* or *MIC60*) and *MDM35* did not lead to strong synthetic defects in growths or CL abundance (Fig. S2A and B), which is in contrast to the case when the *mgm1*Δ*dnm1*Δ and *mdm35*Δ mutations are combined (Figs. 1 and 2). In addition, it should be noted that either MICOS or Mdm35 becomes crucial for crista formation when Mgm1 is absent (*mgm1*Δ*dnm*Δ background) (Fig. 3C, rows 5 and 6). These results clearly indicate that Mgm1 can produce crista structures to some extent even in the absence of both MICOS and Mdm35, yet intramitochondrial PL transport or MICOS alone is not able to produce sufficient crista structures, especially lamellar cristae, in the *mgm1*Δ*dnm1*Δ background. Taken together, we propose that the two distinct pathways that generate crista structures (Fig. 3D); one is the Mgm1-dependent pathway for lamellar crista formation, in which only CJ formation requires the MICOS function (Korner et al. 2009; Harner et al., 2011; Hoppins et al., 2011; von der Malsburg et al., 2011), and the other is the MICOS-dependent pathway for tubular crista formation, in which intramitochondrial PL transport is critical. When either Mgm1- or MICOS-dependent pathway is active, crista structures can be formed. However, simultaneous defects in both the pathways lead to depletion of crista structures, which appears to result in a drastic decrease in the CL levels and severe growth defects (Fig. 3D). The basis that the defective crista formation leads to decreased CL levels will be discussed below.

Compromised mitochondrial fusion/division partly affects the levels of CL synthetic enzymes—PL analyses revealed that the CL level is decreased to about 50% in *fzo1*Δ*dnm1*Δ and *mgm1*Δ*dnm1*Δ cells (Fig. 2). Besides, loss of Mdm35 drastically decreased the CL level in *mgm1*Δ*dnm1*Δ cells whereas it only mildly affected the CL abundance in *fzo1*Δ*dnm1*Δ cells (Fig. 2). A simple explanation for the decreased CL level is that compromised mitochondrial dynamics, as well as abnormal crista morphology, had a negative impact on the stabilities of CL synthetic enzymes. We thus examined the steady-state levels of CL synthetic enzymes in these deletion mutant cells. To detect endogenous levels of Gep4 and Crd1, we chromosomally expressed C-terminally 3xHemagglutinin

(HA)-tagged Gep4 and N-terminally 3xFLAG-tagged Crd1, respectively (Longtine et al., 1998). Immunoblotting of membrane fractions showed that FLAG-Crd1 levels decreased in *fzo1*Δ*dnm1*Δ, *mgm1*Δ*dnm1*Δ, *fzo1*Δ*dnm1*Δ*mdm35*Δ and *mgm1*Δ*dnm1*Δ*mdm35*Δ cells as compared with those in wild-type cells (Fig. 4A). In addition, the levels of Cho2 and Psd1 also decreased in these mutant cells (Fig. 4A), but on the other hand, Tam41 and Gep4-HA levels were comparable or even increased in *fzo1*Δ*dnm1*Δ, *mgm1*Δ*dnm1*Δ, and *mgm1*Δ*dnm1*Δ*mdm35*Δ membranes, as compared with wild-type membranes (Fig. 4A).

The decreased levels of FLAG-Crd1 could explain the decreased CL levels in *fzo1*Δ*dnm1*Δ and *mgm1*Δ*dnm1*Δ cells (Fig. 2). Although *fzo1*Δ*dnm1*Δ and *mgm1*Δ*dnm1*Δ cells are capable of maintaining mtDNA as compared with the single-deletion mutant (*fzo1*Δ and *mgm1*Δ) cells, they (*fzo1*Δ*dnm1*Δ and *mgm1dnm1*Δ cells) still tend to show the ρ^- phenotype more frequently than wild-type cells (Osman et al., 2015). Therefore, compromised respiratory activities arising from the possible accumulation of nonfunctional mtDNA could decrease the membrane potential ($\Delta\Psi$) across the MIM, which would result in defects in the $\Delta\Psi$-requiring MIM and matrix protein import. This is consistent with the previous observation as well as our results that ρ° cells without mtDNA possessed decreased amounts of CL (Chen et al., 2010, Fig. S1). We indeed observed that mitochondria isolated from *fzo1*Δ*dnm1*Δ and *mgm1*Δ*dnm1*Δ cells showed the decreased $\Delta\Psi$ as compared with that of wild-type mitochondria, especially under the fermentable condition (Fig. S3A). In addition, our immunoblotting using mitochondria isolated from cells grown in the nonfermentable (YPLac) medium showed that steady-state levels of FLAG-Crd1 are restored in *fzo1*Δ*dnm1*Δ and *mgm1*Δ*dnm1*Δ mitochondria as compared with those under the fermentable condition (Fig. S3B vs Fig. 4A and F). Consistently, our *in vitro* protein import assay showed that mitochondrial proteins including Crd1 and Psd1 were almost normally imported into *fzo1*Δ*dnm1*Δ and *mgm1*Δ*dnm1*Δ mitochondria isolated under the nonfermentable condition (Fig. S3C). These results suggest that mitochondrial protein import is impaired in *fzo1*Δ*dnm1*Δ and *mgm1*Δ*dnm1*Δ cells due to the decreased $\Delta\Psi$, resulting in the decreased Crd1 levels under the fermentable condition. To further confirm this idea, we assessed the mitochondrial protein import under the fermentable condition *in vivo*. To this end, we forcibly induced the expression of FLAG-Crd1, which is controlled by the *GAL1* promoter, by shifting the growth medium from YPD to YPGal and analyzed the protein levels by immunoblotting. Interestingly, the levels of FLAG-Crd1 were significantly lower in *fzo1*Δ*dnm1*Δ and *mgm1*Δ*dnm1*Δ cells as compared with that in wild-type cells after inducing FLAG-Crd1 expressions (Fig. S3D). We observed similar delayed accumulations of other mitochondrial proteins such as Om45, Cyt c_1, and Kgd1, upon expression in the galactose-containing medium. These observations indeed confirmed our idea that mitochondrial protein import is generally defective in *fzo1*Δ*dnm1*Δ and *mgm1*Δ*dnm1*Δ cells under the fermentable condition. We performed cycloheximide chase experiments using wild-type, *fzo1*Δ*dnm1*Δ and *mgm1*Δ*dnm1*Δ cells overexpressing FLAG-Crd1 from a multi-copy plasmid and found that FLAG-Crd1 and Psd1 were stably present over time in all yeast strains we tested whereas a short-lived protein Fzo1 was rapidly degraded (Escobar-Henriques et al., 2006, Fig. S3E). Therefore, we propose that the general import defect of mitochondrial proteins was the cause of the decreased levels of several mitochondrial proteins including Crd1 in *fzo1*Δ*dnm1*Δ and *mgm1*Δ*dnm1*Δ cells under the

fermentable condition. Although it is still not clear why the level of an ER protein Cho2 decreased and Tam41 and Gep4 levels increased in *fzo1*Δ*dnm1*Δ and *mgm1*Δ*dnm1*Δ cells, transcriptional regulation may contribute to the maintenance of these protein levels.

Similar to Crd1, Psd1, which is anchored to the MIM with its N-terminal transmembrane segment (Horvath et al., 2012), also showed a reduced protein level in *fzo1*Δ*dnm1*Δ and *mgm1*Δ*dnm1*Δ cells, yet without a drastic change in the PE levels (Fig. 2). The only mildly affected level of PE is probably due to the presence of multiple PE synthetic pathways mediated by the endosome-resident PE synthase Psd2, the Kennedy pathway using soluble substrate CDP-ethanolamine and DAG. The amounts of PE methyltransferase Cho2 was also decreased likely as a compensation effect to maintain the normal PE level (Fig. 4A).

Mitochondrial crista formation is prerequisite for normal CL accumulation— Importantly, the observation that CL was hardly present in *mgm1*Δ*dnm1*Δ*mdm35*Δ cells as compared with the *mgm1*Δ*dnm1*Δ and *fzo1*Δ*dnm1*Δ*mdm35*Δ cells (Fig. 2) cannot be ascribed to the decrease in the levels of CL synthetic enzymes because the steady-state levels of CL synthetic enzymes in *mgm1*Δ*dnm1*Δ*mdm35*Δ cells were comparable with those in *mgm1*Δ*dnm1*Δ and *fzo1*Δ*dnm1*Δ*mdm35*Δ cells (Fig. 4A). Rather, these results could be related to significant loss of crista structures in *mgm1*Δ*dnm1*Δ*mdm35*Δ cells, but not in *mgm1*Δ*dnm1*Δ or *fzo1*Δ*dnm1*Δ*mdm35*Δ cells (Fig. 3A). The possibility that decreased CL levels, in turn, result in abnormal crista morphology can be ruled out because the crista structures were not so much affected in *crd1*Δ cells, in which CL was absent (Baile et al., 2014). Therefore, the loss of crista structures appears to negatively affect the CL synthesis and/or maintenance.

To test whether abnormal crista morphology negatively affects the mitochondrial CL abundance, we analyzed the growth and PL compositions of *mgm1*Δ*dnm1*Δ*mic60*Δ cells, in which crista formation would be drastically impaired (Harner et al., 2016). We confirmed that crista structures largely disappeared in *mgm1*Δ*dnm1*Δ*mic60*Δ mitochondria while *fzo1*Δ*dnm1*Δ*mic60*Δ possessed crista tubules without CJs like *mic60*Δ cells (Fig. 4B, C). Like the *mdm35*Δ mutation, the *mic60*Δ mutation also led to severe growth defects and 80% reduction in the CL level for *mgm1*Δ*dnm1*Δ cells as compared with those in wild-type cells whereas it only mildly affected the CL abundance of *fzo1*Δ*dnm1*Δ cells (Fig. 4D, E). In addition, we confirmed that the loss of Mic60 did not affect steady-state levels of CL synthetic enzymes such as Tam41, Gep4, and Crd1 (Fig. 4F). These findings strongly suggest that the abnormality of crista structures causes decreases in the CL levels.

How does the impaired crista formation negatively impact on the CL biogenesis? A simple explanation is that CL is destabilized due to a shortage of the MIM volume as a reservoir of CL if a considerable amount of CL can be synthesized. Another possibility is that CL synthesis itself is impaired when normal crista structures are disrupted. The latter scenario may indicate the presence of a specialized MIM region for CL synthesis, where CL synthetic enzymes, as well as precursor PLs such as PA, CDP-DAG, and PG, are concentrated for efficient PL synthesis. Alternatively, the abnormal MIM structures may disrupt the MOM-MIM contact sites, which would hamper the alternative MOM-to-MIM transfer route for the CL precursor PA that is independent of the Ups1-Mdm35 complex.

STAR★METHODS

CONTACT FOR REAGENT AND RESOURCE SHARING

Further information and requests for resources and reagents should be directed to and will be fulfilled by the Lead Contact, Yasushi Tamura (tamura@sci.kj.yamagata-u.ac.jp).

EXPERIMENTAL MODEL AND SUBJECT DETAILS

In this study, we used a *Saccharomyces cerevisiae* strain, FY833 (MATa *ura3-52 his3*-Δ*200 leu2*-Δ*1 lys2*-Δ*202 trp1*-Δ*63*) as a background strain. All the yeast cells used in this study are listed in the Key Resources Table.

METHOD DETAILS

Strains, plasmids, primers, and growth conditions—Disruption or chromosomal C-terminal tagging of the yeast gene was accomplished by PCR-mediated gene replacement (Longtine et al., 1998) with a pair of primers listed in the KEY RESOURCES TABLE. The *kanMX4* (pBS-*kanMX4*), *hphMX* (pBS-*hphMX*), *HIS3* (pBS-Cg*HIS3*), *URA3* (pRS306) genes were used as disruption markers. For C-terminal HA tagging of *GEP4* gene, the *3xHA-TRP1* gene was amplified by PCR using pFA6a-3xHA-TRP1 as a template (Longtine et al., 1998). For N-terminal FLAG tagging into *CRD1* gene, we used a shuttle vector pAUR135, in which the Aureobasidin A-resistance gene (*AUR1-C*) and *GIN11M86* under the control of *GAL10* promoter were cloned. Since overexpression of GIN11M86 causes growth inhibition, cultivation on galactose-containing media allowed the transformant cells to remove the marker genes from the genomic DNA. (Takara Bio Inc.). Synthetic gene encoding Crd1(1-60)-3xFLAG tag-Crd1(61-283) purchased from Eurofins Genomics was cloned into pAUR135, resulting in pAUR135-FLAG-Crd1. After a single cutting of the plasmid at BglII site present in the N-terminal side of *CRD1*, the resulting linear DNA was introduced into yeast cells and Aureobasidin A-resistance transformants were selected. The transformants were streaked on YPGa1 plate to select marker-removed clones to obtain yeast cells expressing FLAG-Crd1.

A pair of primers, PNU80/81, PNU82/83, PYU674/675, PYU736/737, PYU740/741, PNU1076/1077, or PYU972/973 was used to amplify the gene cassette for *ups1*Δ, *nps2*Δ, *mdm35*Δ, *mic10*Δ, *mic60*Δ, *dnm1*Δ mutation or HA-tagging to the *GEP4* gene, respectively.

To construct pGEM-4Z-Crd1 and pGEM-4Z-Psd1, the *CRD1* and *PSD1* genes were amplified by PCR using the yeast genomic DNA as a template and a pair of primers PYU1550/1551 and PJH189/190, respectively. The *CRD1* and *PSD1* fragments were digested with BamHI/HindIII and SacI/BamHI, and cloned to the multi-cloning site of pGEM-4Z.

Yeast cells were grown in YPD (1% yeast extract, 2% polypeptone, and 2% glucose), YPLac (1% yeast extract, 2% polypeptone, and 3% lactate), YPGal (1% yeast extract, 2% polypeptone, and 3% galactose), SCD (0.67% yeast nitrogen base without amino acids, 0.5% casamino acid, and 2% glucose), SGalSuc (0.67% yeast nitrogen base without amino acids, 2% galactose, and 2% sucrose) supplemented with 20 μg/ml each of adenine, uracil,

L-tryptophan and L-histidine and 30 μg/ml each of L-leucine and L-lysine. YPD supplemented with 200 μg/ml G418, 200 μg/ml Hygromycin B or 100 μg/ml Aureobasidin were used for selection of *kanMX4*, *hphMX6* or *AURa-C*-containing transformants, respectively.

Phospholipid analysis—Yeast cells were diluted to an A_{600} = 0.02 in 1 ml of YPD in the presence of 2 μ Ci/ml $^{32}P_i$ and cultivated to stationary phase. Phospholipids were extracted from total cells and separated by TLC with developing solvent A (chloroform/ethanol/water/triethylamine, 30/35/7/35, v/v) or solvent B (chloroform/methanol/25% ammonia, 65/35/5, v/v) (Tamura et al., 2013). After 2 to 3 hours developing, the TLC plates were dried and sandwiched with storage phosphor screens using an exposure cassette (GE healthcare). The RI-labeled phospholipids were detected by radioimaing with Typhoon FLA-7000 image analyzer (GE Healthcare).

Electron microscopy—For the EM analyses in Fig. 3, yeast cells grown in SGalSuc until early log phase (A_{600} = 0.3 – 0.5) were fixed and embedded in Epon resin, as described (Itoh et al., 2013). Briefly, yeast cells were fixed by perfusing 2% glutaraldehyde, 1 mM $CaCl_2$, and 0.1 M sodium cacodylate, pH 7.2 for 1 hr. After digestion of cell wall by Zymolyase 20T, cells were further fixed in 0.5% osmium teroxide, and 0.8% potassium ferrocyanide. After washing in 0.1 M sodium cacodylate, pH 7.2, cells were embedded in 2.5% low-melting agarose and post-fixed in 1% uranyl acetate for 1.5 hrs. After dehydration using 50, 70, 90, and 100% ethanol and 100% propylene oxide, samples were embedded in Epon resin (Ted Pella). Ultrathin sections were obtained using and Ultracut E (Reichert-Jung, Germany). Sections were stained with 2% uranyl acetate and 3 mg/ml lead citrate, and observed on a Hitachi H-7600 transmission electron microscope (Hitachi, Japan).

For the EM analyses in Fig. 4, yeast cells were fixed by perfusing 2% paraformaldehyde 2% glutaraldehyde, and 0.1 M sodium cacodylate, pH 7.4 at room temperature for 1 h, then transferred to 4°C. The cells were collected and further fixed with 2% glutaraldehyde, and 0.1 M Sodium cacodylate, pH 7.4 at 4°C overnight. After fixation, the samples were washed 3 times with 0.1 M sodium cacodylate, pH 7.4 for 10 min each, and were post-fixed with 1% $KMnO_4$ at room temperature for 2 h. The samples were dehydrated in graded 50% and 70% ethanol solutions for 30 min each at 4°C, 90% for 30 min at room temperature, and then 100% for 30 min at room temperature. The samples were infiltrated with propylene oxide (PO) twice for 30 min each and were put into a 70:30 mixture of PO and resin (Quetol-812; Nisshin EM Co.) for 1 h. PO was volatilized by keeping the cap open overnight. The samples were transferred to a fresh 100% resin, and were polymerized at 60°C for 48 h. The polymerized resins were ultrathin sectioned at 70 nm with a diamond knife using a ultramicrotome (Ultracut UCT, Leica) and the sections were mounted on copper grids. They were stained with 2% uranyl acetate at room temperature for 15 min, and then washed with distilled water followed by being secondary-stained with Lead stain solution (Sigma) at room temperature for 3 min. The grid was observed by a transmission electron microscope (JEM-1400Plus, JEOL) wtih an acceleration voltage of 100 kV. Digital images were taken with a CCD camera (EM014830RUBY2, JEOL).

Isolation of membrane fractions—Yeast cells were cultivated to stationary phase in 50 ml YPD at 30°C. Cells were harvested and incubated in alkaline buffer (0.1 M Tris-HCl, pH 9.5, 10 mM dithiothreitol (DTT)) for 15 min at 30°C. After washing with spheroplast buffer (20 mM Tris-HCl, pH 7.5, 1.2 M sorbitol), the cells were treated with Zymolyase 20T (100 μg/ml final) in spheroplast buffer for 40 min at 30°C. The resulting spheroplasts were re-suspended in ice-cold lysis buffer (20 mM Tris-HCl, pH 7.5, 0.6 M sorbitol, 1 mM phenylmethylsulfonyl fluoride (PMSF)) and frozen in liquid nitrogen. Spheroplasts were then disrupted by rotational vibration at 4,260 rpm for 90 seconds using a cell destroyer PS 1000 (BMS, Japan). After removing unbroken cells by centrifugation at 2,000 × *g* for 5 min, membrane fractions containing mitochondria were precipitated by centrifugation at 15,000 × *g* for 5 min.

Immunoblotting—For immunoblotting, proteins separated on SDS gels were transferred to PVDF membranes (Immobilon-FL or Immobilon-P, Millipore). Then, the membranes were incubated with primary antibodies as stated below and specific proteins were detected by Cy5, Alexa Fluor 488 or HRP-conjugated secondary antibodies, goat anti-rabbit or mouse IgG (H+L) (Thermo Fisher Scientific) and analyzed with Typhoon imager (GE Healthcare) or LAS-4000mini (FUJIFILM Corporation).

Supplementary Material

Refer to Web version on PubMed Central for supplementary material.

Acknowledgments

We thank Kayoko Shishido, Tomomi Sasaki and Michiko Hashimoto for technical assistance and Dr. Yasunori Watanabe for pRS314-GAL-FLAG-Crd1 plasmid. We are grateful to the members of the Tamura, Endo and Sesaki laboratories for valuable discussions. This work was supported by JSPS KAKENHI (Grant Numbers 15H05595 and 17H06414 to YT, and 15H05705 and 22227003 to TE), National Institutes of Health Grants to H.S. (GM123266), AMED-PRIME from Japan Agency for Medical Research and Development, AMED (Grant Number 18gm5910026h0002) (YT), and a CREST Grant from JST (TE).

Reference

Aaltonen MJ, Friedman JR, Osman C, Salin B, di Rago J-P, Nunnari J, Langer T, and Tatsuta T (2016). MICOS and phospholipid transfer by Ups2–Mdm35 organize membrane lipid synthesis in mitochondria. J. Cell Biol 213, 525–534. [PubMed: 27241913]

Baile MG, Sathappa M, Lu Y, Pryce E, Whited K, McCaffery JM, Han X, Alder NN, and Claypool SM (2014). Unremodeled and Remodeled Cardiolipin Are Functionally Indistinguishable in Yeast. J. Biol. Chem 289, 1768–1778. [PubMed: 24285538]

Böttinger L, Horvath SE, Kleinschroth T, Hunte C, Daum G, Pfanner N, and Becker T (2012). Phosphatidylethanolamine and Cardiolipin Differentially Affect the Stability of Mitochondrial Respiratory Chain Supercomplexes. J. Mol. Biol 423, 677–686. [PubMed: 22971339]

Chen S, Liu D, Finley RL, and Greenberg ML (2010). Loss of mitochondrial DNA in the yeast cardiolipin synthase crd1 mutant leads to up-regulation of the protein kinase Swe1p that regulates the G 2/M transition. J. Biol. Chem 285, 10397–10407. [PubMed: 20086012]

Chu CT, Ji J, Dagda RK, Jiang JF, Tyurina YY, Kapralov AA, Tyurin VA, Yanamala N, Shrivastava IH, Mohammadyani D, et al. (2013). Cardiolipin externalization to the outer mitochondrial membrane acts as an elimination signal for mitophagy in neuronal cells. Nat. Cell Biol 15, 1197–1205. [PubMed: 24036476]

Claypool SM, Oktay Y, Boontheung P, Loo JA, and Koehler CM (2008). Cardiolipin defines the interactome of the major ADP/ATP carrier protein of the mitochondrial inner membrane. J. Cell Biol 182, 937–950. [PubMed: 18779372]

Connerth M, Tatsuta T, Haag M, Klecker T, Westermann B, and Langer T (2012). Intramitochondrial Transport of Phosphatidic Acid in Yeast by a Lipid Transfer Protein. Science. 338, 815–818. [PubMed: 23042293]

DeVay RM, Dominguez-Ramirez L, Lackner LL, Hoppins S, Stahlberg H, and Nunnari J (2009). Coassembly of Mgm1 isoforms requires cardiolipin and mediates mitochondrial inner membrane fusion. J. Cell Biol 186, 793–803. [PubMed: 19752025]

Escobar-Henriques M, Westermann B, and Langer T (2006). Regulation of mitochondrial fusion by the F-box protein Mdm30 involves proteasome-independent turnover of Fzo1. J. Cell Biol 173, 645–650. [PubMed: 16735578]

Gebert N, Joshi AS, Kutik S, Becker T, McKenzie M, Guan XL, Mooga VP, Stroud DA, Kulkarni G, Wenk MR, et al. (2009). Mitochondrial Cardiolipin Involved in Outer-Membrane Protein Biogenesis: Implications for Barth Syndrome. Curr. Biol 19, 2133–2139. [PubMed: 19962311]

Gohil VM, Thompson MN, and Greenberg ML (2005). Synthetic lethal interaction of the mitochondrial phosphatidylethanolamine and cardiolipin biosynthetic pathways in Saccharomyces cerevisiae. J. Biol. Chem 280, 35410–35416. [PubMed: 16036913]

Harner M, Körner C, Walther D, Mokranjac D, Kaesmacher J, Welsch U, Griffith J, Mann M, Reggiori F, and Neupert W (2011). The mitochondrial contact site complex, a determinant of mitochondrial architecture. EMBO J. 30, 4356–4370. [PubMed: 22009199]

Harner ME, Unger A-K, Geerts WJ, Mari M, Izawa T, Stenger M, Geimer S, Reggiori F, Westermann B, and Neupert W (2016). An evidence based hypothesis on the existence of two pathways of mitochondrial crista formation. Elife 5, e18853. [PubMed: 27849155]

Hermann GJ, Thatcher JW, Mills JP, Hales KG, Fuller MT, Nunnari J, and Shaw JM (1998). Mitochondrial Fusion in Yeast Requires the Transmembrane GTPase Fzo1p. J. Cell Biol 143, 359–373. [PubMed: 9786948]

Hoppins S, Collins SR, Cassidy-Stone A, Hummel E, DeVay RM, Lackner LL, Westermann B, Schuldiner M, Weissman JS, and Nunnari J (2011). A mitochondrial-focused genetic interaction map reveals a scaffold-like complex required for inner membrane organization in mitochondria. J. Cell Biol 195, 323–340. [PubMed: 21987634]

Horvath SE, Böttinger L, Vögtle F-N, Wiedemann N, Meisinger C, Becker T, and Daum G (2012). Processing and Topology of the Yeast Mitochondrial Phosphatidylserine Decarboxylase 1. J. Biol. Chem 287, 36744–36755. [PubMed: 22984266]

Joshi AS, Thompson MN, Fei N, Hüttemann M, and Greenberg ML (2012). Cardiolipin and mitochondrial phosphatidylethanolamine have overlapping functions in mitochondrial fusion in Saccharomyces cerevisiae. J. Biol. Chem 287, 17589–17597. [PubMed: 22433850]

Kameoka S, Adachi Y, Okamoto K, Iijima M, and Sesaki H (2018). Phosphatidic Acid and Cardiolipin Coordinate Mitochondrial Dynamics. Trends Cell Biol. 28, 67–76. [PubMed: 28911913]

Kutik S, Rissler M, Guan XL, Guiard B, Shui G, Gebert N, Heacock PN, Rehling P, Dowhan W, Wenk MR, et al. (2008). The translocator maintenance protein Tam41 is required for mitochondrial cardiolipin biosynthesis. J. Cell Biol 183, 1213–1221. [PubMed: 19114592]

Lee SM, Chin L-S, and Li L (2012). Charcot-Marie-Tooth disease-linked protein SIMPLE functions with the ESCRT machinery in endosomal trafficking. J. Cell Biol 199, 799–816. [PubMed: 23166352]

Longtine MS, Mckenzie III A, Demarini DJ, Shah NG, Wach A, Brachat A, Philippsen P, and Pringle JR (1998). Additional modules for versatile and economical PCR-based gene deletion and modification in *Saccharomyces cerevisiae*. Yeast 14, 953–961. [PubMed: 9717241]

Malhotra K, Modak A, Nangia S, Daman TH, Gunsel U, Robinson VL, Mokranjac D, May ER, and Alder NN (2017). Cardiolipin mediates membrane and channel interactions of the mitochondrial TIM23 protein import complex receptor Tim50. Sci. Adv 3, e1700532. [PubMed: 28879236]

von der Malsburg K, Müller JM, Bohnert M, Oeljeklaus S, Kwiatkowska P, Becker T, Loniewska-Lwowska A, Wiese S, Rao S, Milenkovic D, et al. (2011). Dual Role of Mitofilin in Mitochondrial Membrane Organization and Protein Biogenesis. Dev. Cell 21, 694–707. [PubMed: 21944719]

Messerschmitt M, lakobs S, Vogel F, Fritz S, Dimmer KS, Neupert W, and Westermann B (2003). The inner membrane protein Mdm33 controls mitochondrial morphology in yeast. J. Cell Biol 160, 553–564. [PubMed: 12591915]

Miyata N, Watanabe Y, Tamura Y, Endo T, and Kuge O (2016). Phosphatidylserine transport by Ups2-Mdm35 in respiration-active mitochondria. J. Cell Biol 214, 77–88. [PubMed: 27354379]

Miyata N, Goda N, Matsuo K, Hoketsu T, and Kuge O (2017). Cooperative function of Fmp30, Mdm31, and Mdm32 in Ups1-independent cardiolipin accumulation in the yeast *Saccharomyces cerevisiae*. Sci. Rep 7, 16447. [PubMed: 29180659]

Osman C, Haag M, Potting C, Rodenfels I, Dip PV, Wieland FT, Brügger B, Westermann B, and Langer T (2009). The genetic interactome of prohibitins: coordinated control of cardiolipin and phosphatidylethanolamine by conserved regulators in mitochondria. J. Cell Biol 184, 583–596. [PubMed: 19221197]

Osman C, Noriega TR, Okreglak V, Fung JC, and Walter P (2015). Integrity of the yeast mitochondrial genome, but not its distribution and inheritance, relies on mitochondrial fission and fusion. Proc. Natl. Acad. Sci 112, E947–E956. [PubMed: 25730886]

Pfeiffer K, Gohil V, Stuart RA, Hunte C, Brandt U, Greenberg ML, and Schagger H (2003). Cardiolipin Stabilizes Respiratory Chain Supercomplexes. J. Biol. Chem 278, 52873–52880. [PubMed: 14561769]

Potting C, Wilmes C, Engmann T, Osman C, and Langer T (2010). Regulation of mitochondrial phospholipids by Ups1/PRELI-like proteins depends on proteolysis and Mdm35. EMBO J. 29, 2888–2898. [PubMed: 20657548]

Rabl R, Soubannier V, Scholz R, Vogel F, Mendl N, Vasiljev-Neumeyer A, Korner C, Jagasia R, Keil T, Baumeister W, et al. (2009). Formation of cristae and crista junctions in mitochondria depends on antagonism between Fcj1 and Su e / g. J. Cell Biol 185, 1047–1063. [PubMed: 19528297]

Sauerwald J, Jores T, Eisenberg-Bord M, Chuartzman SG, Schuldiner M, and Rapaport D (2015). Genome-Wide Screens in *Saccharomyces cerevisiae* Highlight a Role for Cardiolipin in Biogenesis of Mitochondrial Outer Membrane Multispan Proteins. Mol. Cell. Biol 35, 3200–3211. [PubMed: 26149385]

Sesaki H, and Jensen RE (2001). *UGO1* encodes an outer membrane protein required for mitochondrial fusion. J. Cell Biol 152, 1123–1134. [PubMed: 11257114]

Sesaki H, Southard SM, Yaffe MP, and Jensen RE (2003). Mgm1p, a Dynamin-related GTPase, Is Essential for Fusion of the Mitochondrial Outer Membrane. Mol. Biol. Cell 14, 2342–2356. [PubMed: 12808034]

Sesaki H, Dunn CD, Iijima M, Shepard KA, Yaffe MP, Machamer CE, and Jensen RE (2006). Ups1p, a conserved intermembrane space protein, regulates mitochondrial shape and alternative topogenesis of Mgm1p. J. Cell Biol 173, 651–658. [PubMed: 16754953]

Shen Z, Li Y, Gasparski AN, Abeliovich H, and Greenberg ML (2017). Cardiolipin Regulates Mitophagy through the Protein Kinase C Pathway. J. Biol. Chem 292, 2916–2923. [PubMed: 28062576]

Tamura Y, Endo T, Iijima M, and Sesaki H (2009). Ups1p and Ups2p antagonistically regulate cardiolipin metabolism in mitochondria. J. Cell Biol 185, 1029–1045. [PubMed: 19506038]

Tamura Y, Iijima M, and Sesaki H (2010). Mdm35p imports Ups proteins into the mitochondrial intermembrane space by functional complex formation. EMBO J. 29, 2875–2887. [PubMed: 20622808]

Tamura Y, Harada Y, Nishikawa S, Yamano K, Kamiya M, Shiota T, Kuroda T, Kuge O, Sesaki H, Imai K, et al. (2013). Tam41 Is a CDP-Diacylglycerol Synthase Required for Cardiolipin Biosynthesis in Mitochondria. Cell Metab. 17, 709–718. [PubMed: 23623749]

Tarasenko D, Barbot M, Jans DC, Kroppen B, Sadowski B, Heim G, Möbius W, Jakobs S, and Meinecke M (2017). The MICOS component Mic60 displays a conserved membrane-bending activity that is necessary for normal cristae morphology. J. Cell Biol 216, 889–899. [PubMed: 28254827]

Watanabe Y, Tamura Y, Kawano S, and Endo T (2015). Structural and mechanistic insights into phospholipid transfer by Ups1–Mdm35 in mitochondria. Nat. Commun 6, 7922. [PubMed: 26235513]

Winston F, Dollard C, and Ricupero-Hovasse SL (1995) Construction of a set of convenient Saccharomyces cerevisiae strains that are isogenic to S288C. Yeast 11, 53–55 [PubMed: 7762301]

Wong ED, Wagner JA, Gorsich SW, McCaffery JM, Shaw JM, and Nunnari J (2000). The dynamin-related GTPase, Mgm1p, is an intermembrane space protein required for maintenance of fusion competent mitochondria. J. Cell Biol 151, 341–352. [PubMed: 11038181]

Yu F, He F, Yao H, Wang C, Wang J, Li J, Qi X, Xue H, Ding J, and Zhang P (2015). Structural basis of intramitochondrial phosphatidic acid transport mediated by Ups1-Mdm35 complex. EMBO Rep. 76, 813–823.

Zhang M, Mileykovskaya E, and Dowhan W (2005). Cardiolipin is essential for organization of complexes III and IV into a supercomplex in intact yeast mitochondria. J. Biol. Chem 280, 29403–29408. [PubMed: 15972817]

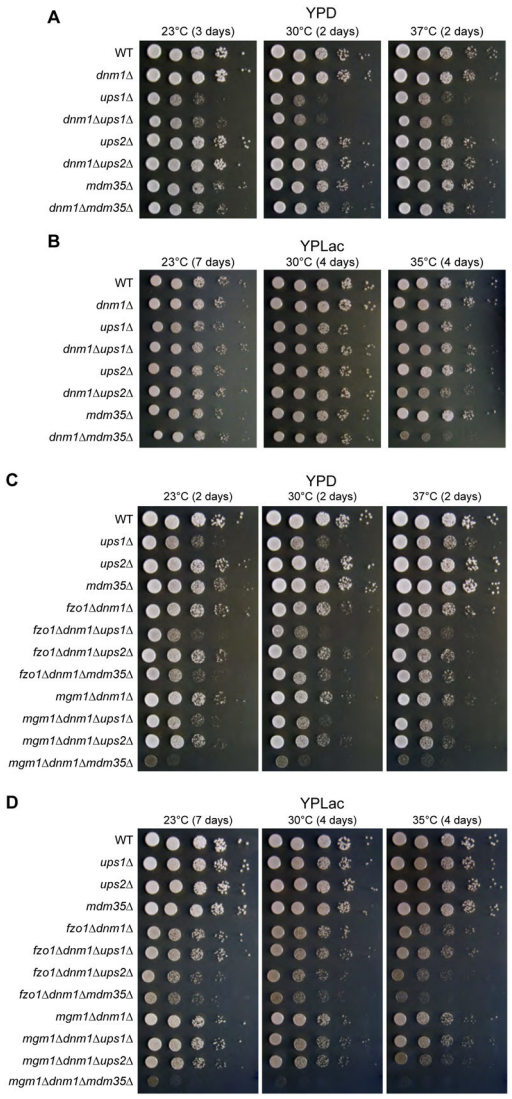

Figure 1. Mdm35 is critical for the growth of the *mgm1Δdnm1Δ* but not *fzo1Δdnm1Δ* strain.
Serial dilutions of the indicated yeast cells were spotted onto (A) (C) YPD or (B) (D) YPLac and cultivated at 23, 30, 37°C (YPD) or 23, 30, 35°C (YPLac) for the indicated time periods.

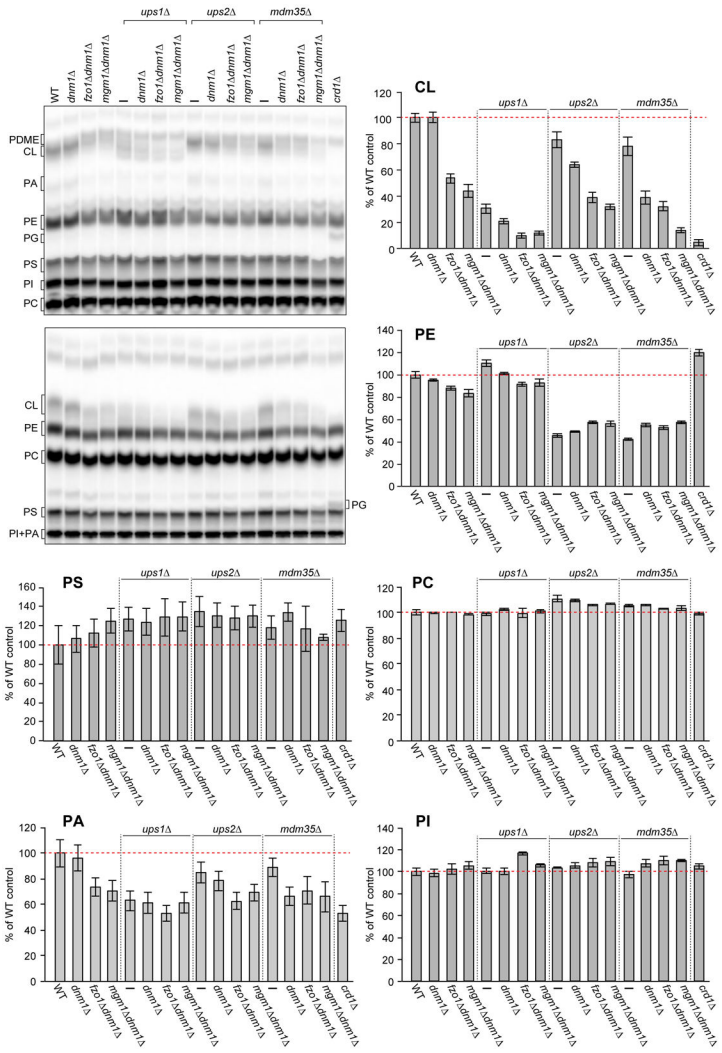

Figure 2. CL level is significantly decreased in the *mgm1Δdnm1Δmdm35Δ* strain.

Indicated yeast cells were grown in YPD media containing 2 μCi/ml ^{32}Pi. Total phospholipids were extracted from whole cells and analyzed by TLC (left panels). Phospholipids were migrated in solvent A (chloroform/ethanol/water/triethylamine, 30/35/7/35, v/v) (top left) and solvent B (chloroform/methanol/25% ammonia, 65/35/5, v/v) (top right). The amounts of CL, PE, PS, PC, PA, and PI were determined (right panels). The ratio of each phospholipid to total phospholipids in wild-type was set to 100%. Values are mean ± SEM (n = 3).

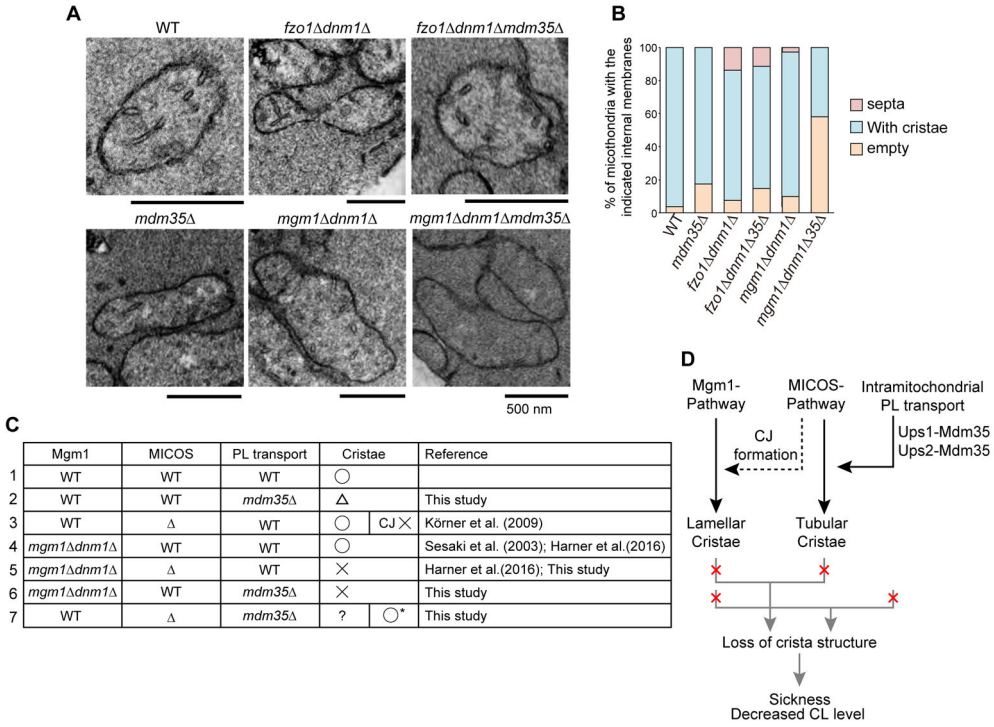

C

	Mgm1	MICOS	PL transport	Cristae		Reference
1	WT	WT	WT	○		
2	WT	WT	*mdm35Δ*	△		This study
3	WT	Δ	WT	○	CJ ×	Körner et al. (2009)
4	*mgm1Δdnm1Δ*	WT	WT	○		Sesaki et al. (2003); Harner et al.(2016)
5	*mgm1Δdnm1Δ*	Δ	WT	×		Harner et al.(2016); This study
6	*mgm1Δdnm1Δ*	WT	*mdm35Δ*	×		This study
7	WT	Δ	*mdm35Δ*	?	○*	This study

Figure 3. The crista formation is drastically impaired in *mgm1Δdnm1Δmdm35Δ* but not in *fzo1Δdnm1mdm35Δ*.

(A) Mitochondria in the indicated yeast cells were observed by TEM. Scale bar: 500 nm (B) About 100 mitochondria were observed for each strain and the ratios of mitochondria with the indicated internal membranes are shown. (C) A summary of relationships among Mgm1, MICOS and Mdm35 functions in crista formation. Δ means lack of MICOS component such as Mic10 or Mic60. “CJ ×” means that CJ formation is defective. ○* means that the growth and CL level are almost normal.

(D) A model of two parallel mechanisms for crista formation.

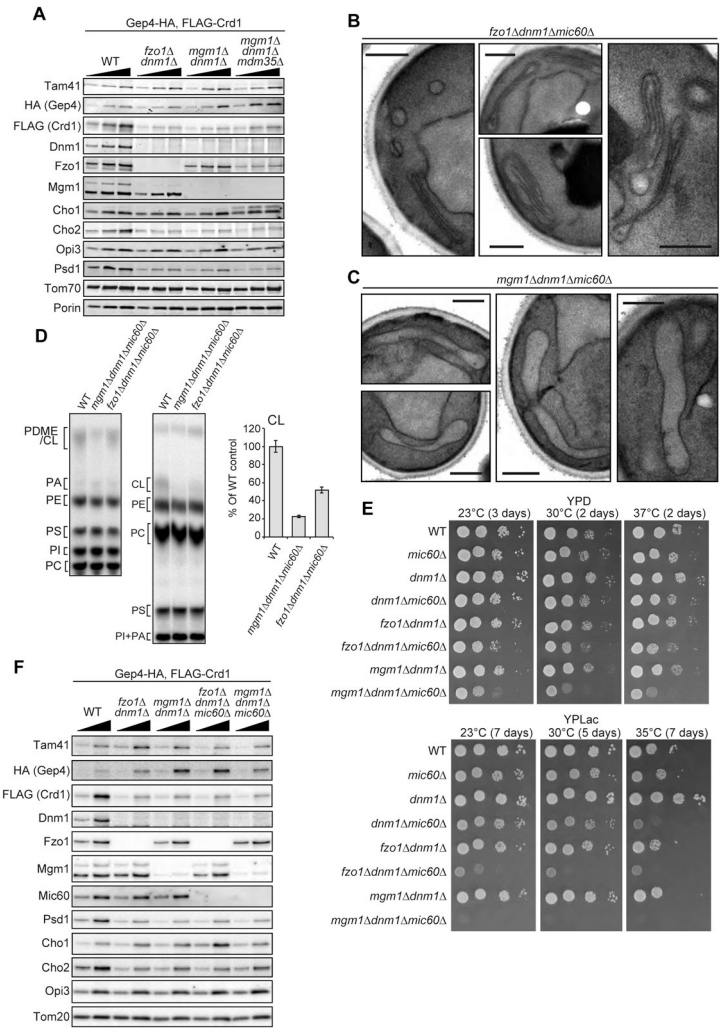

Figure 4. Abnormal crista formation leads to decreased CL levels.

(A) Membrane fractions were extracted from the indicated yeast cells expressing Gep4-HA and FLAG-Crd1 and analyzed by immunoblotting using the indicated antibodies. (B, C) The indicated yeast cells were observed by TEM. Scale bar, 500 nm (D) Total phospholipids prepared from the indicated yeast cells were analyzed by TLC in solvent A (left) or solvent B (right). The CL levels were determined. The ratio of CL to total phospholipids in wild-type cells was set to 100%. Values are mean ± SEM (n = 3). (E) Serial dilutions of the indicated yeast cells were spotted onto YPD or YPLac plates cultivated at 23, 30, 37°C (YPD) or 23, 30, 35°C (YPLac) for the indicated time periods. (F) Membrane fractions were extracted from the indicated yeast cells expressing Gep4-HA and FLAG-Crd1 and analyzed by immunoblotting using the indicated antibodies.

KEY RESOURCES TABLE

REAGENT or RESOURCE	SOURCE	IDENTIFIER
Antibodies		
Rabibit polyclonal anti-Dnm1	Endo Lab	N/A
Rabibit polyclonal anti-Fzo1	Endo Lab	N/A
Rabibit polyclonal anti-Mgm1	Endo Lab	N/A
Rabibit polyclonal anti-Tam41	Endo Lab	N/A
Rabibit polyclonal anti-Cho1	Endo Lab	N/A
Rabibit polyclonal anti-Cho2	Tamura Lab	N/A
Rabibit polyclonal anti-Opi3	Sesaki Lab	N/A
Rabibit polyclonal anti-Psd1	Tamura Lab	N/A
Rabibit polyclonal anti-Tom70	Sesaki Lab	N/A
Rabibit polyclonal anti-Tom40	Endo Lab	N/A
Rabibit polyclonal anti-Tom20	Endo Lab	N/A
Rabibit polyclonal anti-Tim23	Endo Lab	N/A
Rabibit polyclonal anti-Tim44	Endo Lab	N/A
Rabibit polyclonal anti-Pam16	Endo Lab	N/A
Rabibit polyclonal anti-Pam18	Endo Lab	N/A
Rabibit polyclonal anti-Kgd1	Endo Lab	N/A
Rabibit polyclonal anti-Ssc1	Endo Lab	N/A
Rabibit polyclonal anti-Mdj1	Endo Lab	N/A
Rabibit polyclonal anti-Om45	Endo Lab	N/A
Rabibit polyclonal anti-Cytb_2	Endo Lab	N/A
Rabibit polyclonal anti-Cytc_1	Endo Lab	N/A
Rabibit polyclonal anti-$F_1\beta$	Endo Lab	N/A
Rabibit polyclonal anti-Porin	Endo Lab	N/A
Rabibit polyclonal anti-Mic60	Endo Lab	N/A
Rabibit polyclonal anti-HA	MBL Lifescience	Cat# M180-3;
		RRID:AB_10951811
ANTI-FLAG M2 Monoclonal Antibody	Sigma-Aldrich	Cat# F3165; RRID:AB_259529
Cy5 AffiniPure Goat Anti-Rabbit IgG (H+L)	Jackson ImmunoResearch Labs	Cat# 111-175-144; RRID:AB_2338013
Goat anti-Mouse IgG1 Secondary Antibody, Alexa Fluor 488 conjugate	Thermo Fisher Scientific	Cat# A-21121, RRID:AB_2535764
Goat anti-Rabbit IgG (H+L) Cross-Adsorbed Secondary Antibody, HRP	Thermo Fisher Scientific	Cat# A16104, RRID:AB_2534776)
Goat anti-Mouse IgG (H+L) Cross-Adsorbed Secondary Antibody, HRP	Thermo Fisher Scientific	Cat# A16072; RRID:AB_2534745
Bacterial and Virus Strains		
XL2-blue	N/A	N/A

REAGENT or RESOURCE	SOURCE	IDENTIFIER
Chemicals, Peptides, and Recombinant Proteins		
Valinomycin	Wako	Cat# 228-01121
JC-1	Thermo Fisher Scientific	Cat# T3168
Zymolyase-20T	Nakalai tesque	Cat# 07663-91
TnT® Quick Coupled Transcription/Translation System	Promega	Cat# L1170
Met-35S-Label, [L-Methionine 35S+L-Cysteine 35S]	American Radiolabeled Chemicals Inc.	Cat# ARS0110
NADH	Sigma-Aldrich	Cat# N8129
ATP	Sigma-Aldrich	Cat# A7699
BSA fatty acid free	Nakalai tesque	Cat# 08587-26
Cycloheximide	Wako	Cat# 037-20991
TLC plates (SILGUR-25-C UV_{254})	MACHEREY-NAGEL	Cat# 810123
PVDF membrane (Immobilon-P)	Merck-Millipore	Cat# IPVH00010
PVDF membrane (Immobilon-FL)	Merck-Millipore	Cat# PFL00010
Experimental Models: Organisms/Strains		
All listed below are *Saccharomyces cerevisiae* strains		
FY833- MATa *ura3-52 his3-Δ200 leu2-Δ1 lys2-Δ202 trp1-Δ63*	Winston et al., 1995	N/A
FY833 ρ°- MATa *ura3-52 his3-Δ200 leu2-Δ1 lys2-Δ202 trp1-Δ63* ρ°	This study	N/A
*dnm1*Δ- MATa *ura3-52 his3-Δ200 leu2-Δ1 lys2-Δ202 trp1-Δ63 dnm1Δ::URA3*	This study	N/A
*ups1*Δ- MATa *ura3-52 his3-Δ200 leu2-Δ1 lys2-Δ202 trp1-Δ63 ups1Δ::kanMX4*	Sesaki et al., 2006	N/A
*dnm1Δups1*Δ- MATa *ura3-52 his3-Δ200 leu2-Δ1 lys2-Δ202 trp1-Δ63 dnm1*Δ::URA3 ups1Δ::kanMX4	This study	N/A
*ups2*Δ- MATa *ura3-52 his3-Δ200 leu2-Δ1 lys2-Δ202 trp1-Δ63* ups2A::HIS3	Tamura et al., 2009	N/A
*dnm1Δups2*Δ- MATa *ura3-52 his3-Δ200 leu2-Δ1 lys2-Δ202 trp1-Δ63 dnm1*Δ::URA3 ups2A::HIS3	This study	N/A
*mdm35*Δ- MATa *ura3-52 his3-Δ200 leu2-Δ1 lys2-Δ202 trp1-Δ63 mdm35Δ::URA3*	Tamura et al., 2010	N/A
*dnm1Δmdm35*Δ- MATa *ura3-52 his3-Δ200 leu2-Δ1 lys2-Δ202 trp1-Δ63 dnm1Δ::kanMX4 mdm35Δ::HIS3*	This study	N/A
*fzo1*Δ- MATa *ura3-52 his3-Δ200 leu2-Δ1 lys2-Δ202 trp1-Δ63 fzo1Δ::kanMX4*	This study	N/A
*fzo1Δdnm1*Δ- MATa *ura3-52 his3-Δ200 leu2-Δ1 lys2-Δ202 trp1-Δ63 fzo1Δ::kanMX4 dnm1Δ::kanMX4*	Sesaki et al., 2006	N/A
*fzo1Δdnm1Δups1*Δ- MATa *ura3-52 his3-Δ200 leu2-Δ1 lys2-Δ202 trp1-Δ63 fzo1Δ::kanMX4 dnm1Δ::kanMX4 ups1Δ::HIS3*	This study	N/A
*fzo1Δdnm1Δups2*Δ- MATa *ura3-52 his3-Δ200 leu2-Δ1 lys2-Δ202 trp1-Δ63 fzo1Δ::kanMX4 dnm1Δ::kanMX4 ups2Δ::HIS3*	This study	N/A
*fzo1Δdnm1Δmdm35*Δ- MATa *ura3-52 his3-Δ200 leu2-Δ1 lys2-Δ202 trp1-Δ63 fzo1Δ::kanMX4 dnm1Δ::kanMX4 mdm35Δ::HIS3*	This study	N/A
*mgm1*Δ- MATa *ura3-52 his3-Δ200 leu2-Δ1 lys2-Δ202 trp1-Δ63 mgm1Δ::kanMX4*	This study	N/A
*mgm1Δdnm1*Δ- MATa *ura3-52 his3-Δ200 leu2-Δ1 lys2-Δ202 trp1-Δ63 mgm1Δ::kanMX4 dnm1Δ::kanMX4*	Sesaki et al., 2006	N/A
*mgm1Δdnm1Δups1*Δ- MATa *ura3-52 his3-Δ200 leu2-Δ1 lys2-Δ202 trp1-Δ63 mgm1Δ::kanMX4 dnm1Δ::kanMX4 ups1Δ::HIS3*	This study	N/A

REAGENT or RESOURCE	SOURCE	IDENTIFIER
mgm1Δdnm1Δups2Δ- MATa *ura3-52 his3-Δ200 leu2-Δ1 lys2-Δ202 trp1-Δ63 mgm1Δ::kanMX4 dnm1Δ::kanMX4 ups2Δ::HIS3*	This study	N/A
mgm1Δdnm1Δmdm35Δ- MATa *ura3-52 his3-Δ200 leu2-Δ1 lys2-Δ202 trp1-Δ63 mgm1Δ::kanMX4 dnm1Δ::kanMX4 mdm35Δ::HIS3*	This study	N/A
mic60Δ- MATa *ura3-52 his3-Δ200 leu2-Δ1 lys2-Δ202 trp1- Δ63 mic60Δ::hphMX*	This study	N/A
mic60Δmdm35Δ- MATa *ura3-52 his3-Δ200 leu2-Δ1 lys2-Δ202 trp1-Δ63 mic60Δ::hphMX mdm35Δ::kanMX4*	This study	N/A
mic10Δ- MATa *ura3-52 his3-Δ200 leu2-Δ1 lys2-Δ202 trp1-Δ63 mic10Δ::hphMX*	This study	N/A
mic10Δmdm35Δ- MATa *ura3-52 his3-Δ200 leu2-Δ1 lys2-Δ202 trp1-Δ63 mic10Δ::hphMX mdm35Δ::kanMX4*	This study	N/A
dnm1Δmic60Δ- MATa *ura3-52 his3-Δ200 leu2-Δ1 lys2-Δ202 trp1-Δ63 dnm1Δ::kanMX4 mic60Δ::hphMX*	This study	N/A
crd1Δ- MATa *ura3-52 his3-Δ200 leu2-Δ1 lys2-Δ202 trp1-Δ63 dnm1Δ::kanMX4 crd1Δ::kanMX4*	This study	N/A
fzo1Δdnm1Δmic60Δ- MATa *ura3-52 his3-Δ200 leu2-Δ1 lys2-Δ202 trp1-Δ63 fzo1Δ::kanMX4 dnm1Δ::kanMX4 mic60Δ::hphMX*	This study	N/A
mgm1Δdnm1Δmic60Δ- MATa *ura3-52 his3-Δ200 leu2-Δ1 lys2-Δ202 trp1-Δ63 mgm1Δ::kanMX4 dnm1Δ::kanMX4 mic60Δ::hphMX*	This study	N/A
Gep4-HA FLAG-Crd1- MATa *ura3-52 his3-Δ200 leu2-Δ1 lys2-Δ202 trp1-Δ63 GEP4-3HA::TRP1 3FLAG-CRD1*	This study	N/A
Gep4-HA FLAG-Crd1 fzo1Δdnm1Δ- MATa *ura3-52 his3-Δ200 leu2-Δ1 lys2-Δ202 trp1-Δ63 GEP4-3HA::TRP1 3FLAG-CRD1 fzotΔ::kanMX4 dnm1Δ::kanMX4*	This study	N/A
Gep4-HA FLAG-Crd1 mgm1Δdnm1Δ- MATa *ura3-52 his3-Δ200 leu2-Δ1 lys2-Δ202 trp1-Δ63 GEP4-3HA::TRP1 3FLAG-CRD1 mgm1Δ::kanMX4 dnm1Δ::kanMX4*	This study	N/A
Gep4-HA FLAG-Crd1 mgm1Δdnm1Δmdm35Δ- MATa *ura3-52 his3-Δ200 leu2-Δ1 lys2-Δ202 trp1-Δ63 GEP4-3HA::TRP1 3FLAG-CRD1 mgm1Δ::kanMX4 dnm1Δ::kanMX4 mdm35::HIS3*	This study	N/A
Gep4-HA FLAG-Crd1 fzo1Δdnm1Δmic60Δ- MATa *ura3-52 his3-Δ200 leu2-Δ1 lys2-Δ202 trp1-Δ63 GEP4-3HA::TRP1 3FLAG-CRD1 fzo1Δ::kanMX4 dnm1Δ::kanMX4 mic60Δ::hphMX*	This study	N/A
Gep4-HA FLAG-Crd1 mgm1Δdnm1Δmic60Δ- MATa *ura3-52 his3-Δ200 leu2-Δ1 lys2-Δ202 trp1-Δ63 GEP4-3HA::TRP1 3FLAG-CRD1 mgm1Δ::kanMX4 dnm1Δ::kanMX4 mic60Δ::hphMX*	This study	N/A
Oligonucleotides		
AGTATTGTCTGGCTTCTGAGACGGCGGTAAGATATCCTTAAGAGTTGCAAGATTGTACTGAGAGTGCAC	This study	PNU80
CAATTTCGCTCGCCCATGGTGATATCTTTAAAGATCTTTAAATGGGAACACTGTGCGGTATTTCACACCG	This study	PNU81
AATAGATTTCAGACTAAGATAAAATAATCGAGAATAATTAAAAGACGATAAGATTGTACTGAGAGTGCAC	This study	PNU82
AGGAATATAAGTAGTATGCAGTGCCATGCGGGATCAAGGAATTTGTATCTCTGTGCGGTATTTCACACCG	This study	PNU83
GAGTTTATCATTAAGTAGCTACCAGCGAATCTAAATACGACGGATAAAGAGTTGTAAAACGACGGCCAGT	This study	PNU1076
ATCACGCCCGCAATGTTGAAGTAAGATCAAAAATGAGATGAATTATGCAACACAGGAAACAGCTATGACC	This study	PNU1077
ATCTGTTTGTGTTTTAACTTGAATTACAATAACAATAATACCAGTTTTATGTTGTAAAACGACGGCCAGT	This study	PYU674
ATTAGTATTTACATGTTGAATAATGCACATTCTGTGCTAAAATATATACTCACAGGAAACAGCTATGACC	This study	PYU675
ATTAACTTTGCTACGAGAGGGAATAAACACGGAAAAAGACAAAATATACCGTTGTAAAACGACGGCCAGT	This study	PYU736
ATTTTTATTATTTTTTTTTTTGAATATATATAAAGCATCGTCGCTTAAGACACAGGAAACAGCTATGACC	This study	PYU737
ACACAAAAGGCATAAGAACGCATTGAAAAGTCTAAAAAACTAATATTCGTGTTGTAAAACGACGGCCAGT	This study	PYU740
GGAAATTGAGGTGTAATGACGTACATCTCTTTTCTCTTTGTATTATTCTTCACAGGAAACAGCTATGACC	This study	PYU741
CTCCAAGTTCGAAAAAAAATTATACAACTTTTTGGGATTTCGGATCCCCGGGTTAATTAA	This study	PYU972
AAAAAATTAAAATGTTTTACTTTTTATTAAAGTTGCCTAAGAATTCGAGCTCGTTTAAAC	This study	PYU973
AATTGGATCCAATTTAGTCAATGATTCAAATGG	This study	PYU1550
CAGTAAGCTTCTATTTTAAAAGTTTAAAAGCG	This study	PYU1551
CCCCGAGCTCCGCTCAAATCCTTCTTGGTCGTTATT	This study	PJH189

REAGENT or RESOURCE	SOURCE	IDENTIFIER
CCCCGGATCCTCATTTTAAATCATTCTTTCCAATTATG	This study	PJH190
Recombinant DNA		
pBS-*kanMX4*	Endo Lab	N/A
pBS-*hphMX*	Endo Lab	N/A
pBS-*CgHIS3*	Endo Lab	N/A
pGEM-4Z	Promega	Cat#: P2161
pGEM-4Z-Crd1	This study	N/A
pGEM-4Z-Psd1	This study	N/A
pGEM-4Z-Hsp60	Tamura et al., 2009	N/A
pGEM-4Z-Tim23	Tamura et al., 2009	N/A
pGEM-4Z-AAC	Tamura et al., 2009	N/A
pFA6a-3xHA-TRP1	Longtine et al., 1998	N/A
pAUR135	Takara Bio Inc.	N/A
pAUR135-FLAG-Crd1	This study	N/A
pRS314-GAL1-FLAG-Crd1	This study	N/A